中图法分类号: TP391.41　　**文献标志码**: A　　**文章编号**: 1006-8961(2011)12-2223-08
论文索引信息: Yu Yuanpo, Pan Zhenkuan, Wei Weibo, Jiang Jing. Comparison of the edge preservation capabilities of different variational models for vectorial image denoising [J]. 中国图象图形学报, 2011, 16(12): 2223-2230

Comparison of the edge preservation capabilities of different variational models for vectorial image denoising

Yu Yuanpo, Pan Zhenkuan, Wei Weibo, Jiang Jing
(*College of Information Engineering, Qingdao University, Qingdao* 266071 *China*)

Abstract: Variational models for vectorial image denoising involve couplings of different channels to preserve edges, which lead to problems of complexity and efficiency. Meanwhile, different types of couplings result in different edge preserving effects. The objective of our work is to design fast Split-Bregman algorithms for a couple of variational models which have been proposed in recent years and compare their edge preserving properties and their efficiency. Five variational models for vectorial image denoising using different regularizers are studied: the LTV (layered total variation) regularizer, the MTV (multichannel total variation) regularizer, the CTV (color total variation) regularizer, the PA (polyakov action) regularizer, and the RPA (reduced polyakov action) regularizer. The order of their edge preserving quality and computation efficiency are given based on numerical experiments. It is shown that the CTV model is the best method for edge preserving followed by the PA model, the MTV model, the RPA model, and the LTV model. The LTV model is the fastest model, followed by the MTV model, the RPA model, the CTV model, and the PA model.

Keywords: vectorial images; variational models; edge preserving; image denoising; Split-Bregman algorithm

几种矢量图像噪声去除变分模型的边缘保持比较

于远坡,潘振宽,魏伟波,蒋静
(青岛大学信息工程学院,青岛　266071)

摘　要: 矢量图像噪声去除的变分模型必须考虑不同通道图像间的耦合以保持图像边缘,但所得到的模型复杂、计算效率低,且不同耦合方法对应的模型的边缘保持质量不同。本文首先设计了目前已经提出的这类变分模型的快速 Split Bregman 算法,然后通过大量数值实验对不同模型的边缘保持特性和计算效率进行了比较。所研究的模型分别使用 LTV(layered total variation)规则项、MTV(multichannel total variation)规则项、CTV(color total variation)规则项、PA(polyakov action)规则项和 RPA(reduced polyakov action)规则项。实验结果表明 CTV 模型对矢量图像去噪边缘保持最好,其他依次是 PA 模型、MTV 模型、RPA 模型和 LTV 模型;LTV 模型计算效率最高,其他依次是 MTV 模型、RPA 模型、CTV 模型和 PA 模型。

关键词: 矢量图像;变分模型;边缘保持;图像去噪;Split-Bregman 算法

0　Introduction

Edge preserving is a basic requirement for noise removal tasks in image processing, which has been solved successfully for scalar image denoising using variational models, such as the TV (total variation)

收稿日期: 2011-05-27; **修回日期**: 2011-09-30
基金项目: 国家自然科学基金项目(61170106)。
第一作者简介: 于远坡(1986—　),男。青岛大学信息工程学院计算机应用技术专业硕士研究生,主要研究方向为图像处理。E-mail: yuanpo_yu@126.com

model[1], anisotropic diffusion models[2], and the models based on Riemannian geometry[3]. But they cannot be applied directly to denoise vectorial images because it will lead to smearing edges due to the ignorance of the couplings of different layers of the images.

In order to overcome this problem, Sapiro and Ringach[4] proposed the anisotropic regularizer in the variational function based on the eigenvalues and eigenvectors of the structure tensor of vectorial images to diffuse the images along edges. Inspired by reference [1,4], Blomgren and Chan[5] proposed the CTV (color total variation) model using the Euclidean norm as regularizer. Aujol & Kang[6] and Yang et al[7] proposed a simplified version of reference [5], which is named MTV (multi-channel total variation) model. Bresson & Chan[8] and Duval et al[9], named their model VTV (vector total variation) model and expressed its regularizer in dual form. Another important variational model was proposed by refervence [10-12], based on Polyakov action under the Riemannian framework which is named PA (Polyakov action) model in this paper. Its reduced version can be obtained via missing the cross multiplication terms in the regularizer of the PA model, which is named RPA model here. Although the models mentioned above are claimed by different authors considering the couplings between different channels of vectorial images to reduce the smearing effects on edges, their results have not yet been compared.

Due to the complexity of the regularization terms in the variational models for noise removal of vectorial images, the computation schemes based on the traditional gradient descent equations[8] are slow. The fast dual method[13] cannot be extended to all cases. Therefore we design Split-Bregman algorithms[14] for all the models mentioned above to simplify their implementation and speed up their computation. This is the second goal of our work here.

1 Introduction to the split-Bregman algorithm of TV model

The Split-Bregman algorithm, proposed by Goldstein and Osher[14], combines the fast Split method[15] and the Bregman iterative method[16] for the image restoration problem. The following TV model is used for scalar image denoising

$$\min_{u}\left\{E(\boldsymbol{u}) = \int_{\Omega} |\nabla \boldsymbol{u}| \, dx + \frac{\lambda}{2}\int_{\Omega}(\boldsymbol{u}-\boldsymbol{f})^2 dx\right\} \quad (1)$$

where $\boldsymbol{f}$ is the original image intensity defined in the domain $\boldsymbol{\Omega}$, $\boldsymbol{u}$ is the desired image to be found, and λ is the penalty parameter. By introducing the auxiliary variable $\boldsymbol{w}$ and the Bregman iterative parameter $\boldsymbol{b}$, Goldstein and Osher[14] transform Eq. (1) into the following Split-Bregman iterative formulation:

$$(u^{k+1}, w^{k+1}) = \arg\min_{u,w}(E(u,w)) = \int_{\Omega} |\boldsymbol{w}| \, dx + \frac{\lambda}{2}\int_{\Omega}(\boldsymbol{u}-\boldsymbol{f})^2 dx + \frac{\theta}{2}\int_{\Omega}(\boldsymbol{w}-\nabla \boldsymbol{u}-\boldsymbol{b}^{k+1})^2 dx) \quad (2)$$

where, $b^{k+1} = b^k + \nabla u^k - w^k$ and $b^0 = w^0 = 0$. Using the alternating minimization method, one can obtain the Euler-Lagrange equations on u with

$$\begin{cases}\lambda(\boldsymbol{u}-\boldsymbol{f}) + \theta\nabla\cdot(w^k - \nabla \boldsymbol{u} - b^{k+1}) = 0 & \text{in } \boldsymbol{\Omega} \\ (w^k - \nabla u - b^{k+1})\cdot \boldsymbol{n} = 0 & \text{on } \partial\boldsymbol{\Omega}\end{cases} \quad (3)$$

After u^{k+1} is obtained in an iterative loop, w^{k+1} can be solved via the following generalized soft thresholding formula:

$$w^{k+1} = \max\left(|\nabla u^{k+1} + b^{k+1}| - \frac{1}{\theta}, 0\right)\times \frac{\nabla u^{k+1} + b^{k+1}}{|\nabla u^{k+1} + b^{k+1}|} \quad (4)$$

$$0\cdot\frac{0}{0} = 0$$

where, $0\cdot\frac{0}{0} = 0$ means if $\nabla u^{k+1} + b^{k+1} = 0$, then $w^{k+1} = 0$. Eq. (3) can be solved using the Gauss-Seidel iteration. Eq. (4) is in closed form, and both can be implemented easily and with high efficiency.

2 Split-Bregman algorithms for various vectorial image denoising models

2.1 The Split-Bregman algorithm for the LTV model

The simplest variational vectorial image denoising model can be considered as the direct application of the

TV model for scalar image denoising to its different layers. If the vectorial image with n channels is $\boldsymbol{f} = \{f_1, f_2, \cdots, f_n\}$, the desired restored image is $\boldsymbol{u} = \{u_1, u_2, \cdots, u_n\}$ and the LTV (layered total variation) model using LTV regularizer can be stated as:

$$\min_u \{E(\boldsymbol{u}) = \sum_{i=1}^{n} \int_{\boldsymbol{\Omega}} |\nabla u_i| \,\mathrm{d}x + \frac{\lambda}{2} \sum_{i=1}^{n} \int_{\boldsymbol{\Omega}} (u_i - f_i)^2 \mathrm{d}x\} \tag{5}$$

By introducing an auxiliary variable w and the Bregman iterative parameter $\boldsymbol{b}$, Eq. (5) can be transformed into the following Split-Bregman iterative formulation:

$$(u^{k+1}, w^{k+1}) = \arg\min_{u,w} \Big\{ E(\boldsymbol{u}, \boldsymbol{w}) = \sum_{i=1}^{n} \int_{\Omega} |w_i| \,\mathrm{d}x + \frac{\lambda}{2} \sum_{i=1}^{n} \int_{\Omega} (u_i - f_i)^2 \mathrm{d}x + \frac{\theta}{2} \sum_{i=1}^{n} \int_{\Omega} (w_i - \nabla u_i - b_i^{k+1})^2 \mathrm{d}x \Big\} \tag{6}$$

In each iterative step, u^{k+1} and w^{k+1} can be obtained by solving the following Euler-Lagrange equations and generalized soft thresholding formulas

$$\begin{cases} \lambda(u_i - f_i) + \theta \nabla \cdot (w_i^k - \nabla u_i - b_i^{k+1}) = 0 & \text{in } \boldsymbol{\Omega} \\ (w_i^k - \nabla u_i - b_i^{k+1}) \cdot \boldsymbol{n} = 0 & \text{on } \partial \boldsymbol{\Omega} \end{cases} \tag{7}$$

$$w_i^{k+1} = \max\left(|\nabla u_i^{k+1} + b_i^{k+1}| - \frac{1}{\theta}, 0 \right) \times \frac{\nabla u_i^{k+1} + b_i^{k+1}}{|\nabla u_i^{k+1} + b_i^{k+1}|} \tag{8}$$

$$0 \cdot \frac{0}{0} = 0$$

2.2 The Split-Bregman algorithm for the MTV model

Using the MTV regularizer proposed by reference [9-10, 16-17], the minimization problem for vectorial image denoising can be stated as:

$$\min_u \Big\{ E(u) = \int_{\boldsymbol{\Omega}} \sqrt{\sum_{i=1}^{n} |\nabla u_i|^2} \mathrm{d}x + \frac{\lambda}{2} \sum_{i=1}^{n} \int_{\Omega} (u_i - f_i)^2 \mathrm{d}x \Big\} \tag{9}$$

By introducing an auxiliary variable w and the Bregman iterative parameter $\boldsymbol{b}$, Eq. (9) can be cast into the following Split-Bregman iterative formulation:

$$(u^{k+1}, w^{k+1}) = \arg\min_{u,w} \Big\{ E(\boldsymbol{u}, \boldsymbol{w}) = \int_{\boldsymbol{\Omega}} \sqrt{\sum_{i=1}^{n} |w_i|^2} \mathrm{d}x + \frac{\lambda}{2} \sum_{i=1}^{n} \int_{\Omega} (u_i - f_i)^2 \mathrm{d}x + \frac{\theta}{2} \sum_{i=1}^{n} \int_{\Omega} (w_i - \nabla u_i - b_i^{k+1})^2 \mathrm{d}x \Big\} \tag{10}$$

In each iterative step, u^{k+1} and w^{k+1} can be obtained by solving the following Eq. (7) and generalized soft thresholding formulas.

$$w_i^{k+1} = \max\left(|\nabla u_i^{k+1} + b_i^{k+1}| - \frac{1}{\theta} \frac{|w_i^k|}{\sqrt{\sum_{i=1}^{n} |w_i^k|^2}}, 0 \right) \times \frac{\nabla u_i^{k+1} + b_i^{k+1}}{|\nabla u_i^{k+1} + b_i^{k+1}|} \tag{11}$$

with $0 \cdot \frac{0}{0} = 0$.

2.3 The Split-Bregman algorithm for the CTV model

Using the CTV regularizer proposed in reference [5] the minimization problem for vectorial image denoising can be stated as:

$$\min_u \Big\{ E(u) = \sqrt{\sum_{i=1}^{n} \left(\int_{\Omega} |\nabla u_i| \mathrm{d}x \right)^2} + \frac{\lambda}{2} \sum_{i=1}^{n} \int_{\Omega} (u_i - f_i)^2 \mathrm{d}x \Big\} \tag{12}$$

By introducing an auxiliary variable w and the Bregman iterative parameter $\boldsymbol{b}$, Eq. (12) can be transformed into the following Split-Bregman iterative formulation.

$$(u^{k+1}, w^{k+1}) = \arg\min_{u,w} \Big\{ E(u, w) = \sqrt{\sum_{i=1}^{n} \left(\int_{\Omega} |w_i| \mathrm{d}x \right)^2} + \frac{\lambda}{2} \sum_{i=1}^{n} \int_{\Omega} (u_i - f_i)^2 \mathrm{d}x + \frac{\theta}{2} \sum_{i=1}^{n} \int_{\Omega} (w_i - \nabla u_i - b_i^{k+1})^2 \mathrm{d}x \Big\} \tag{13}$$

In each iterative step, u^{k+1} and w^{k+1} can be obtained by solving Eq. (7) and the following generalized soft thresholding formulas.

$$w_i^{k+1} = \max\Big(|\nabla u_i^{k+1} + b_i^{k+1}| - \frac{1}{\theta} \times$$

$$\left.\frac{\int_{\Omega}|w_i^k|\mathrm{d}x}{\sqrt{\sum_{i=1}^{n}\left(\int_{\Omega}|w_i^k|\mathrm{d}x\right)^2}},0\right)\times\frac{\nabla u_i^{k+1}+b_i^{k+1}}{|\nabla u_i^{k+1}+b_i^{k+1}|} \quad (14)$$

with $0\cdot\frac{0}{0}=0$.

2.4 The Split-Bregman algorithm for the variational model based on the PA regularizer

Using the regularizer based on Polyakov action (PA) proposed in reference[10-12], the minimization problem for vectorial image denoising can be stated as:

$$\min_{u}\left\{E(\boldsymbol{u})=\int_{\Omega}\sqrt{1+\beta^2\sum_{i=1}^{n}|\nabla u_i|^2+\frac{\beta^4}{2}\sum_{i=1,j=1}^{n}|\nabla u_i\times\nabla u_j|^2}\mathrm{d}x+\frac{\lambda}{2}\sum_{i=1}^{n}\int_{\Omega}(u_i-f_i)^2\mathrm{d}x\right\} \quad (15)$$

By introducing an auxiliary variable w and the Bregman iterative parameter b, Eq. (15) can be transformed into the following Split-Bregman iterative formulation:

$$(u^{k+1},w^{k+1})=\arg\min_{u,w}\left\{E(\boldsymbol{u},\boldsymbol{w})=\int_{\Omega}\sqrt{1+\beta^2\sum_{i=1}^{n}|w_i|^2+\frac{\beta^4}{2}\sum_{i=1,j=1}^{n}|w_i\times w_j|^2}\mathrm{d}x+\frac{\lambda}{2}\sum_{i=1}^{n}\int_{\Omega}(u_i-f_i)^2\mathrm{d}x+\frac{\theta}{2}\sum_{i=1}^{n}\int_{\Omega}(w_i-\nabla u_i-b_i^{k+1})^2\mathrm{d}x\right\} \quad (16)$$

In each iterative step, u^{k+1} and w^{k+1} can be obtained by solving Eq. (7) and the following Euler-Lagrange equations

$$w_i^{k+1}=\left[\theta(\nabla u_i^{k+1}+b_i^{k+1})\left(1+\beta^2\sum_{l=1}^{n}|w_l^k|^2+\frac{\beta^4}{2}\sum_{l=1,j=1}^{n}|w_l^k\times w_j^k|\right)^{1/2}-\frac{\beta^4}{2}\sum_{j=1}^{n}(w_i^k\times w_j^k)\times w_j^k\right]\Big/\left(\beta^2+\theta\sqrt{1+\beta^2\sum_{l=1}^{n}|w_l^k|^2+\frac{\beta^4}{2}\sum_{l=1,j=1}^{n}|w_l^k\times w_j^k|^2}\right) \quad (17)$$

For the reduced Polyakov action (RPA) regularizer, the corresponding variational image denoising model is

$$\min_{u}\left\{E(u)=\int_{\Omega}\sqrt{1+\sum_{i=1}^{n}|\nabla u_i|^2}\mathrm{d}x+\frac{\lambda}{2}\sum_{i=1}^{n}\int_{\Omega}(u_i-f_i)^2\mathrm{d}x\right\} \quad (18)$$

By introducing an auxiliary variable w and the Bregman iterative parameter b, Eq. (18) can be transformed into the following Split-Bregman iterative formulation:

$$(u^{k+1},w^{k+1})=\arg\min_{u,w}\left\{E(u,w)=\int_{\Omega}\sqrt{1+\sum_{i=1}^{n}|w_i|^2}\mathrm{d}x+\frac{\lambda}{2}\sum_{i=1}^{n}\int_{\Omega}(u_i-f_i)^2\mathrm{d}x+\frac{\theta}{2}\sum_{i=1}^{n}\int_{\Omega}(w_i-\nabla u_i-b_i^{k+1})^2\mathrm{d}x\right\} \quad (19)$$

In each iterative step, u^{k+1} and w^{k+1} can be obtained by solving Eq. (7) and the following generalized soft thresholding formulas

$$w_i^{k+1}=\max\left(|\nabla u_i^{k+1}+b_i^{k+1}|-\frac{|w_i^k|}{\theta\sqrt{1+\sum_{i=1}^{n}|w_i^k|^2}},0\right)\times\frac{\nabla u_i^{k+1}+b_i^{k+1}}{|\nabla u_i^{k+1}+b_i^{k+1}|} \quad (20)$$

with $0\cdot\frac{0}{0}=0$.

3 Numerical Examples

In order to compare the edge preserving performance and the computational efficiency of different variational models for vectorial image denoising, a color image composed of four color bars with different Gauss noises is used for the first denoising tests. All experiments in this section are implemented using Matlab 7.0 on a PC (Intel (R), CPU 2.0 GHz, with 2 GB memory).

Fig. 1(a) shows the reference color bar image, while Fig. 1(b) shows three local regions around different edges, and Fig. 1(c) shows an image with Gauss noise whose mean and variance are 0 and 0.01 respectively. Fig. 2—6 present the denoising results using the LTV, MTV, CTV, PA, and RPA models respectively, demonstrating different edge preserving effects. Table 1 compares the iterative steps and the time used for convergence.

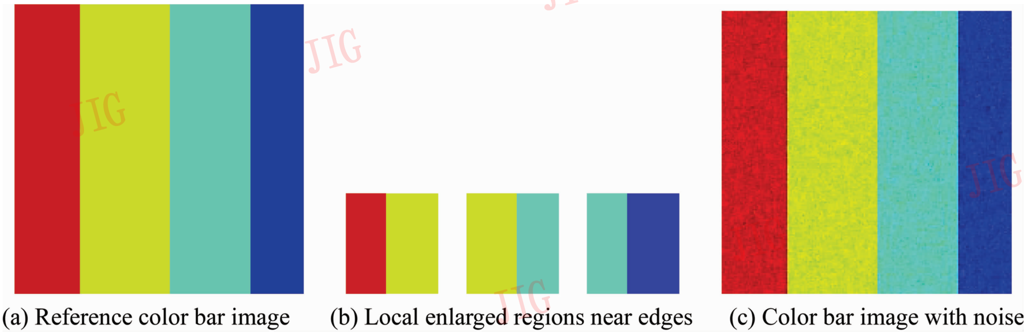

Fig. 1　Color bar images with and without noise

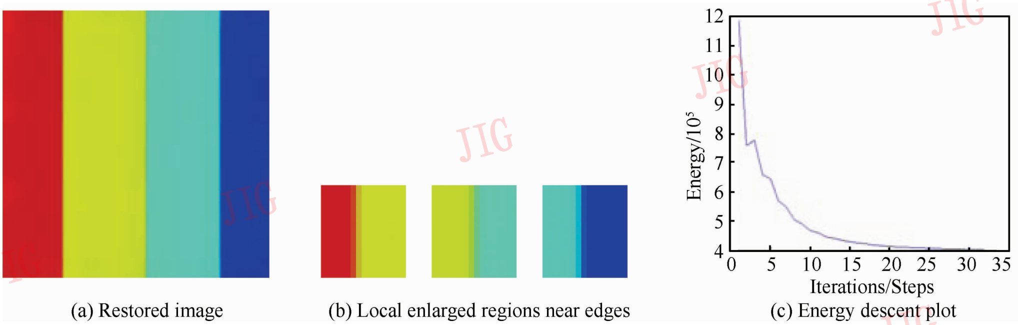

Fig. 2　Denoising results using the LTV model

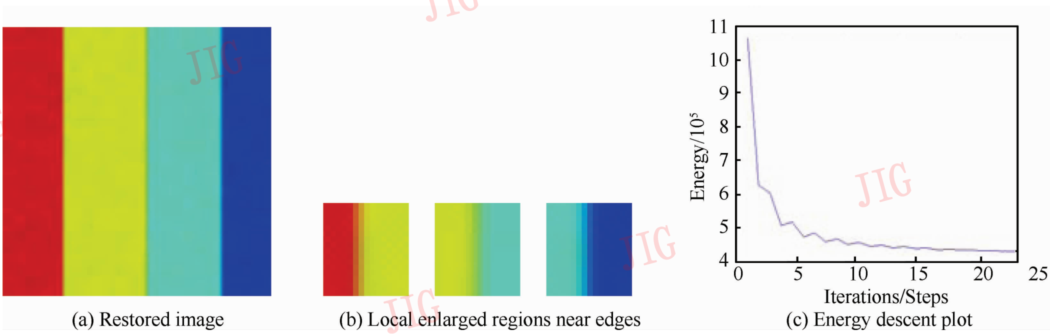

Fig. 3　Denoising results using the MTV model

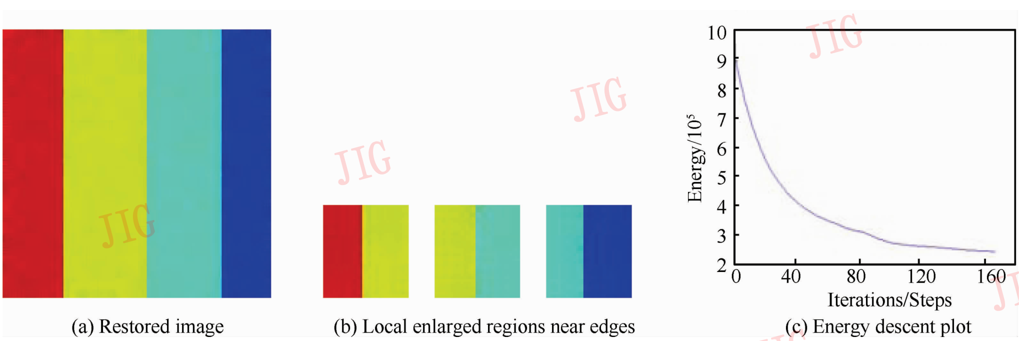

Fig. 4　Denoising results using the CTV model

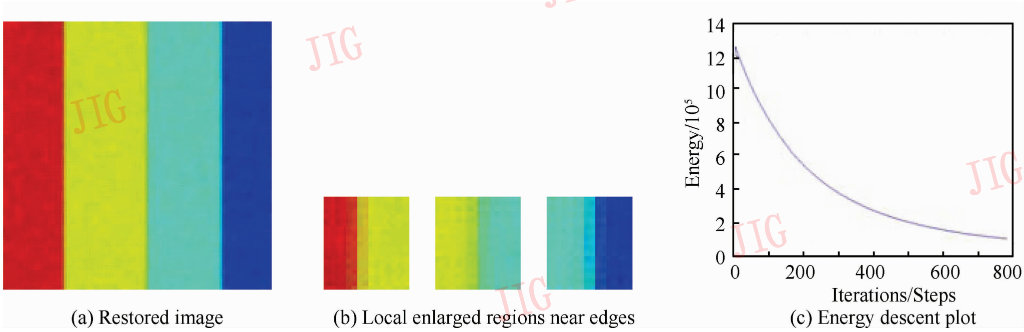

Fig. 5　Denoising results using the PA model

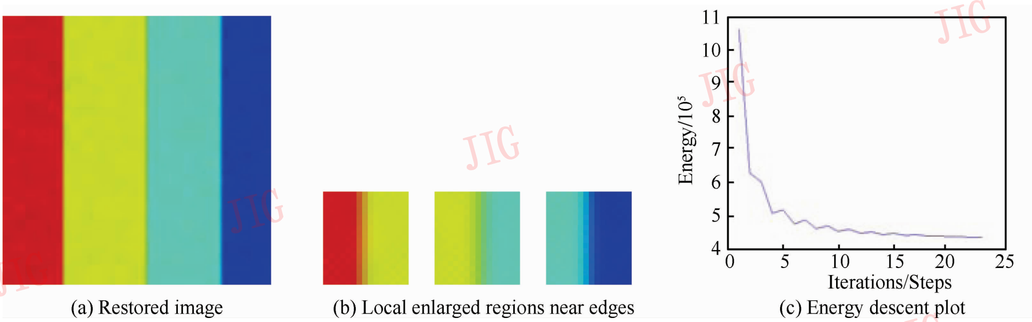

Fig. 6　Denoising results using the RPA model

Tab. 1　Comparison of the efficiency of the different models

	LTV	MTV	CTV	PA	RPV
Parameters (λ/θ)	0.01 /0.02	0.01/0.2	0.01/0.000 3	0.01/0.000 02(β = 10)	0.01/0.2
Errors/Steps	0.001/34	0.001/25	0.001/169	0.002/785	0.001/23
Time/s	2.062	3.804	13.391	52.235	3.640

Fig. 7　presents a color bar image with Gauss noise whose mean and variance are 0 and 0.05 respectively.

Fig. 8(a) shows a local region near an edge of the reference image, Fig. 8(b)—(f) present different edge preserving effects of the denoising results using the LTV, MTV, CTV, PA, and RPA models respectively. Table 2 compares the iterative steps and the time used for convergence.

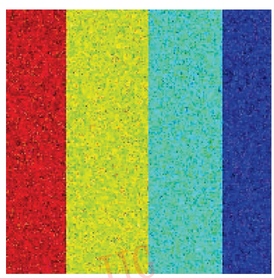

Fig. 7　A color bar image with Gauss noise

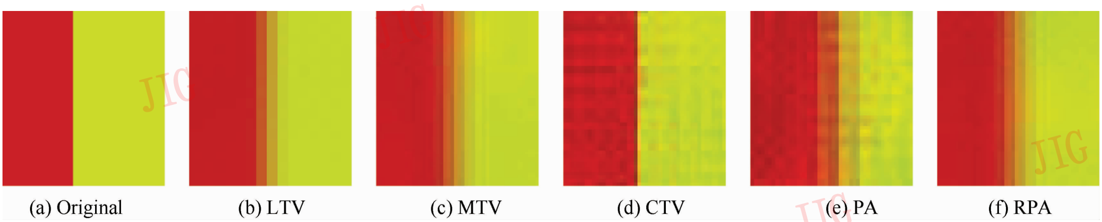

Fig. 8　Edge preserving effects of different models

Tab. 2　Comparison of the efficiency of the different models

	LTV	MTV	CTV	PA	RPV
Parameters (λ/θ)	0.008 /0.05	0.008/0.2	0.008/0.000 2	0.008/0.000 02(β = 10)	0.008/0.2
Errors/Steps	0.001/59	0.001/31	0.001/182	0.002/883	0.001/31
Time/s	3.797	4.734	14.025	57.844	4.891

Fig. 9 presents the reference color mark image and the image noised with Gauss noise with mean 0 and variance 0.01. Fig. 10 shows the denoising results using the LTV, MTV, CTV, PA, and RPA models respectively. Table 3 compares the efficiency of the different models.

Our additional experiments, which we cannot present here due to the page limit, also lead to the same conclusion:

1) The order of denoising ability is: LTV, MTV, RPA, CTV, and PA.

2) The order of edge preserving ability is: CTV, PA, MTV, RPA, and LTV.

3) The order of computation efficiency is: LTV, MTV, RPA, CTV, and PA.

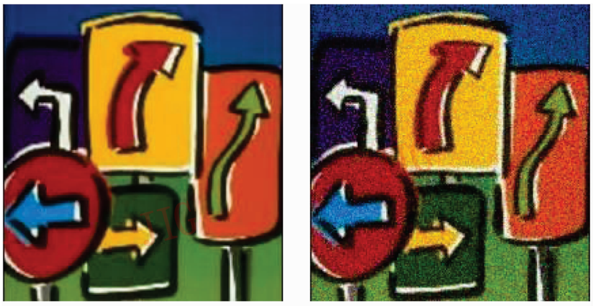

(a) Reference color mark image　(b) Noisy color mark image

Fig. 9　Color mark images with and without noises

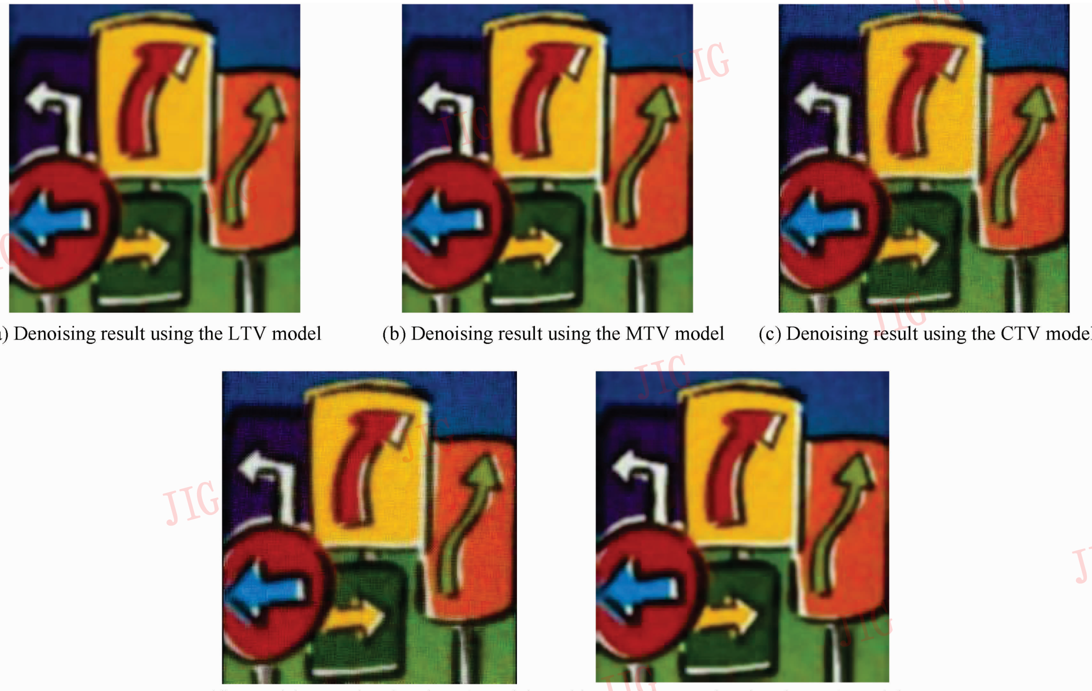

(a) Denoising result using the LTV model　(b) Denoising result using the MTV model　(c) Denoising result using the CTV model

(d) Denoising result using the PA model　(e) Denoising result using the RPA model

Fig. 10　Denoising results using different models

Tab. 3　Comparison of the efficiency of different models

	LTV	MTV	CTV	PA	RPV
Parameters (λ/θ)	0.01 /0.8	0.01/0.2	0.01 /0.000 4	0.01 /0.000 1(β = 10)	0.01/0.2
Errors/Steps	0.01 /23	0.01/11	0.01/ 29	0.01/127	0.01/11
Time/s	1.875	2.109	2.781	11.848	2.078

4 Concluding Remarks

The nonlinear variational diffusion models for scalar image denoising with edge preserving are successful, but they cannot be applied to vectorial image denoising with edge preserving directly due to the different diffusion effects on different channels. The edge preserving capabilities of five vectorial image denoising variational models are compared based on their Split-Bregman algorithms in this paper using the same penalty parameters. Their computing efficiency and denoising effects on flat areas are also compared. Because different models may need different penalty parameters to achieve the best denoising results for different images, some additional conclusions may be made based on further investigations on the effects of the penalty parameters.

References

[1] Rudin L, Osher S, Fatemi E. Nonlinear total variation based noise removal algorithms [J]. Physica D, 1992, 60(1-4):259-268.

[2] Weickert J. Theoretical foundations of anisotropic diffusion in image processing [J]. Computing Supplement, 1996, 11:221-236.

[3] Sochen N, Kimmel R, Malladi R. A general framework for low level vision [J]. IEEE Transactions on Image Processing, Special Issue on PDE based Image Processing, 1998, 7(3):310-318.

[4] Sapiro G, Ringach D L. Anisotropic Diffusion of Multi-valued Images with Applications to Color Filtering [J]. IEEE Transactions on Image Processing, 1996, 5(11): 1582-1586.

[5] Blomgren P, Chan T F. Color TV: Total variation methods for restoration of vector-valued images [J]. IEEE Trans. Image Processing, 1998, 7:304-309.

[6] Aujol J F, Kang S H. Color Image Decomposition and Restoration [J]. Journal of Visual Communication and Image Representation, 2006: 17(4): 916-928.

[7] Yang J, Yin W, Zhang Y. A fast algorithm for edge-preserving variational multichannel image restoration [J]. SIAM Journal on Imaging Sciences, 2009, 2(2):569-592.

[8] Bresson X, Chan T F. Fast dual minimization of the vectorial total variation norm and applications to color image processing [J]. Inverse Problems and Imaging, 2008, 2:455-484.

[9] Duval V, Aujol J F, Vese L, A Projected Gradient Algorithm for Color Image Decomposition [R/OL]. [2011-04-03]. http://hal.archives-ouvertes.fr/hal-00292898.

[10] Brook A, Kimmel R, Sochen N. Variational restoration and edge detection for color images [J]. J. Math. Imaging Vision, 2003, 18:247-268.

[11] Bar L, Brook A, Sochen N, et al. Deblurring of color images corrupted by impulsive noise [J]. IEEE Trans. Image Process, 2007, 16 (4):1101-1111.

[12] Kaftory R, Sochen N, Yehushua Y Z. Variational blind deconvolution of multi-channel images [J]. IJIST, 2005, 1(15):56-63.

[13] Chambolle A. An algorithm for total variation minimization and applications [J]. J. Math. Imag. Vis., 2004, 20: 89-97.

[14] Goldstein T, Osher S. The Split Bregman algorithm for L1 regularized problems [J]. SIAM Journal on Imaging Sciences, 2009, 2(2):323-343.

[15] Wang Y, Yang J, Yin W, et al. A new alternating minimization algorithm for total variation image reconstruction [J] SIAM Journal on Imaging Sciences, 2008, 1(3):248-272.

[16] Osher S, Burger M, Goldfarb D, et al. An iterative regularization method for total variation-based image restoration [J]. SIAM Journal on Multiscale Modeling and Simulation, 2005, 4(2):460-489.